PERGAMON

International Journal of Solids and Structures 38 (2001) 4357–4374

INTERNATIONAL JOURNAL OF SOLIDS and STRUCTURES

www.elsevier.com/locate/ijsolstr

Response of piezoelectric stack actuators under combined electro-mechanical loading

Milan Mitrovic [a,*], Greg P. Carman [a], Friedrich K. Straub [b]

[a] *Department of Mechanical and Aerospace Engineering, University of California, 48-121 Eng. IV, Los Angeles, CA 90095 USA*
[b] *Boeing, M30-B346, 5000E. McDowell Road, Mesa, AZ 85215, USA*

Received 24 August 1999; in revised form 2 June 2000

Abstract

The response of six piezoelectric stack actuators under electrical, mechanical, and combined electro-mechanical loading was investigated. The focus was to understand the behavior of piezoelectric materials under combined electro-mechanical loading scenario, and to determine fundamental properties necessary to model the constitutive response and optimize the actuator performance. Parameters that were evaluated include strain output, permittivity, mechanical stiffness, energy density, and coupling coefficients as a function of mechanical preload and electric field values. Results indicate that for certain actuators stiffness values change by more than 100% depending on the operating conditions. The magnitude of the applied compressive load significantly influences strain output, electrical and mechanical energy density, and coupling coefficients. Initially, the strain output and energy density is enhanced with an increase in mechanical preload by as much as 60% for some actuators, with maximum values occurring at preloads between 25 and 40 MPa. A similar trend is observed under combined out-of-phase electro-mechanical loading. However, linear superposition of strain outputs obtained under constant loading tests, does not lead to accurate predictions over the broad range of combined electro-mechanical loading conditions. This indicates a need for more accurate constitutive relations to predict the highly non-linear processes related to combined electro-mechanical loading.

Keywords: Piezoelectric stacks; Coupling coefficients; Energy density; Electro-mechanical loading

1. Introduction

Piezoelectric materials are currently being investigated in a number of actuator applications, including precision positioning, vibration suppression, noise control, and compact hybrid actuator devices (Sumali et al., 1992; Chen et al., 1998). Another application that has received considerable attention in recent years

* Corresponding author. Tel.: +1-310-825-9564; fax: +1-310-206-4830.
E-mail address: milanx@cad.ucla.edu (M. Mitrovic).

0020-7683/01/$ - see front matter
PII: S0020-7683(00)00273-0

Nomenclature

D	electric flux
d_{33}	piezoelectric coefficient
E	Young's modulus
E	applied electric field
e_r	relative permittivity
k^2	coupling coefficient
f	cyclic frequency
U_E	electrical energy density (energy delivered to the actuator)
U_M	mechanical energy density (energy delivered by the actuator)
ε	strain
$\Delta\sigma$	cyclic stress amplitude
ρ	density of the material

is the active control of helicopter rotor vibration (Lee and Chopra, 1998; Prechtl and Hall, 1998; Straub and Merkley, 1995). Analytical models suggest that 90% of the vibration load imparted to the hub can be alleviated with an active control flap (Friedman and Millott, 1995) positioned on the outboard rear section of the blade. To achieve this, many designs that incorporate active materials have been investigated with different functional requirements (Prechtl and Hall, 1998; Straub and Merkley, 1995). Due to the limited displacement capabilities of piezoelectric actuators, one must evaluate and model the material's response under conditions simulating operating environments to maximize their output.

Initially, piezoelectric materials were developed for high-frequency, low-displacement acoustic applications (Giurgiutiu, 1995). Therefore, a large amount of data is available in the literature that focuses on electro-thermo-mechanical behavior of piezoelectric materials for sensor related issues, i.e., high frequency, low electric field values, and low mechanical loads. This is inappropriate for actuator applications which are intended for use at higher electric fields, lower frequencies, and larger mechanical loads. Furthermore, due to inherent non-linearities at these load and field levels, elastic and piezoelectric properties supplied by stack manufacturers are insufficient to accurately model the response of these materials. Also, properties of stack actuators under the combined electro-mechanical loading are not readily available, and they are the main focus of this study.

In this paper, we experimentally evaluate the response of several piezoelectric stack actuators under electrical, mechanical, and combined electro-mechanical loading. Properties that were directly measured include strain output, permittivity, mechanical stiffness, energy density, and coupling coefficients as a function of mechanical loading parameters and electric field values. Results are presented for PZT-5H and PZT-5A types of materials as well as PLZT compositions. The objective is to determine the optimum operating conditions, and provide basic property measurements to the solid and structure community. Results indicate that certain operating conditions (i.e., mechanical prestress) can improve actuation capabilities by enhancing these properties. For example, strain output was found to increase by 60% for some actuators with compressive prestress. This is mainly due to the contribution of the extrinsic material properties on the overall piezoelectric response, i.e., non-180° domain wall motion. However, in the case when the material is used to achieve large displacements through domain wall motion, another important feature that needs to be addressed is long-term fatigue. This is especially important since electro-mechanical fatigue can degrade the electro-mechanical properties of the material (Wang et al., 1998). Since fatigue

related issues were not the focus of this study, test procedures and results presented in this paper should be viewed as guide to conduct future electro-mechanical fatigue tests.

2. Material characterization

Piezoelectric epoxy-bonded stacks were used in this study, and the properties of these actuators are listed in Table 1. Samples were obtained from different manufacturers, and they include both PZT-5H and PZT-5A types of materials as well as PLZT compositions (Table 1). Stack nomenclature as indicated in this table (Stacks A–F) will be used throughout this paper when the performance of these actuators is described. It should be noted that different electrical loading conditions were used for each stack. Maximum electric field values that are listed in Table 1 correspond to manufacturer's recommended values. Minimum electric fields were chosen as 20% of the suggested maximum field value, sufficiently far from the coercive field values. One sample from each manufacturer is evaluated in this study, except for Sumitomo Stack B for which average properties of two samples are presented.

All tests were conducted in a 100 kN Instron 8516 servo-hydraulic test frame at room temperature, and the illustration of the experimental setup is shown in Fig. 1. When mechanically loading the sample, compliant layers were placed between the sample and compression platens to provide both insulation and to equally distribute load on the sample (i.e., prevent misalignment during compression loading). In addition, measurements of two axial strain gages adhesively bonded to opposite sides of the specimens were compared to assure that bending does not occur. The strain readings were collected using high-speed signal conditioning amplifiers (Vishays). Trek high voltage amplifiers were used to apply the electric field (voltage) and a Wavetek-29 function generator supplied the control signal (sine wave). Actuators free stroke was also measured using LVDT to assure that the actuator's coating to which strain gages were bonded did not influence strain measurements. All data presented in this paper are from the strain gauge readings. Load applied by the test frame, strain readings from strain gages, and current and voltage output from the high voltage amplifier were recorded during each test. Three types of tests were performed for each stack:

Table 1
Piezoelectric stack nomenclature and properties

Stack	A	B	C	D	E	F
Manufacturer	Physik Instrumente	Sumitomo	Rockwell Science Center	Rockwell Science Center	TRS Ceramics Inc.	TRS Ceramics Inc.
Material	PZT	PZT-5H	PLZT	PLZT-9	TRS600FG (PZT-5H equiv.)	TRS200FG (PZT-5A equiv.)
Actuator area	10×10 mm^2	12.2×12.2 mm^2	12.7×12.7 mm^2	10.2×10.2 mm^2	$d = 10$ mm	$d = 10$ mm
Actuator height (mm)	18.03	18.03	18.03	20.32	13.72	14.35
Active region (mm)	15.75	17.27	16.51	19.30	12	12
Plate thickness (mm)	0.104	0.109	0.267	0.406	0.5	0.5
Maximum voltage (V)	120	150	540	800	1000	1000
Minimum voltage (V)	−24	−30	−110	−160	−200	−200
Maximum electric field (MV/m)	1.16	1.38	2.01	1.96	2.00	2.00
Minimum electric field (MV/m)	−0.23	−0.28	−0.40	−0.39	−0.40	−0.40
Capacitance (μF)	8	9	1.1	0.58	0.09	0.07
d_{33} (m/V)	984×10^{-12}	N/A	N/A	N/A	565×10^{-12}	365×10^{-12}
Young's modulus E (GPa)	31	N/A	N/A	N/A	52	60
Density (kg/m^3)	7700	8160	7800	7750	7750	7700

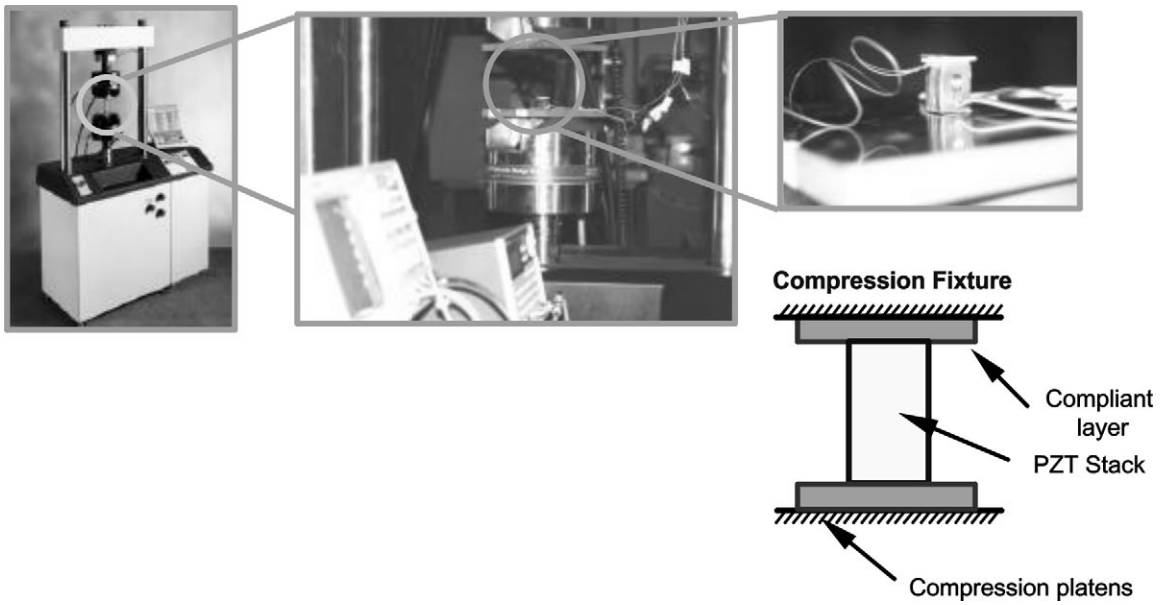

Fig. 1. Experimental setup.

1. mechanical loading at constant electric field,
2. electrical loading at constant mechanical load,
3. combined electro-mechanical loading.

2.1. Mechanical loading

Mechanical characterization tests were performed under different constant electrical conditions and for different values of operating compressive stress range. Electrical conditions include constant flux (open-circuit) and constant electric field. Tests under the constant electric field were conducted at three different values of the applied electric field: 0, 1/2 max, and under the *maximum* manufacturer's recommended electric field. After the application of constant electric field, mechanical load was applied to the sample (sine wave). Mechanical load ranges that were evaluated include 0–55.2 MPa (0–8 ksi) and 0–68.9 MPa (0–10 ksi). Measurements were performed at different cycling frequencies for the load range of 0–68.9 MPa, i.e., 0.1, 1, 10, and 40 Hz. An example of the compression stress–strain response (Stack B) at different electrical loading conditions is shown in Fig. 2. Also included in this figure are the values of Young's modulus, E, calculated for specific load range, i.e., slope of the stress–strain curve between 13.8 and 41.4 MPa (2 and 6 ksi). While the data presented in Fig. 2 are for one specific loading frequency (0.1 Hz), it should be pointed out that the loading frequency did not significantly influence mechanical properties (0.1–40 Hz) for all stacks.

It can be seen from Fig. 2 that stiffness of the piezoelectric stack is influenced by the value of applied electric field, and it generally increases with an increase in the applied electric field. Also, the slope of the stress–strain curve changes significantly as a function of the applied load range. This is especially prominent for the first loading cycle under short-circuit conditions (Fig. 2(a)). In this case, a large residual strain (hysteresis) is observed that was not present when a sufficiently large electric field was applied (Fig. 2(b)). The general trend in data indicates that stiffness increases by more than 50% for certain actuators, as the

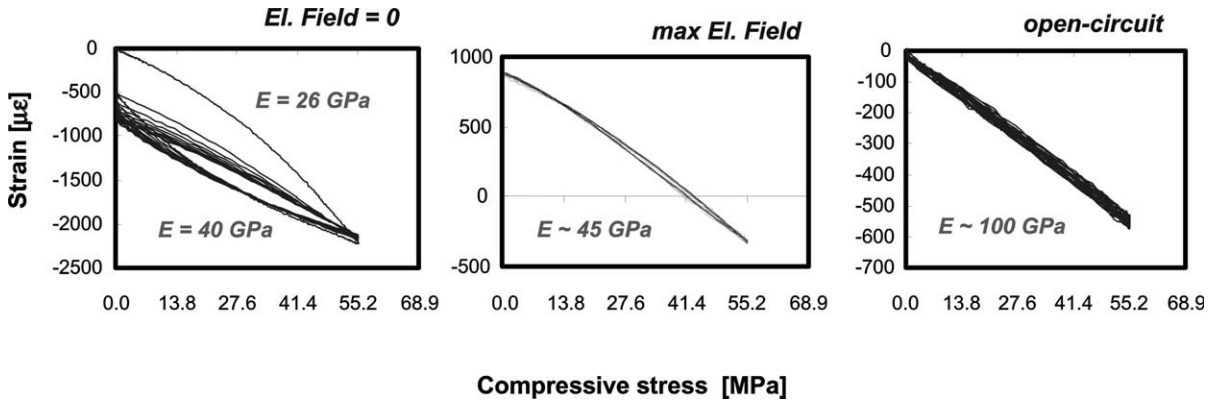

Fig. 2. Stress–strain response as a function of applied electric field (Stack B, 10 mechanical cycles at 0.1 Hz).

field level increases. Similar behavior is observed by Park et al. (1998) for ferro-electric single crystals, and is attributed to non-180° domain wall motion. Without an applied electric field these domains easily rotate perpendicular to the direction of applied mechanical load, and they will stay in that position after the removal of external load, leading to hysteresis. This behavior results in different stiffness properties during the first and subsequent loading cycles (Fig. 2(a)). However, at higher electric fields these domains remain aligned parallel to the applied electric field, and larger mechanical loads are required to re-orient them perpendicular to the load direction. Therefore, the elastic displacement is smaller when an electric field is applied to the system leading to a more stiff system.

In actuator applications, piezoelectric stacks will be cycled between minimum and maximum operational electric fields. Since actuator's Young's modulus depends on the applied electric field (Fig. 2), its stiffness properties will go through periods of lower stiffness (under small electric field) to periods of higher stiffness (large electric field) during each cycle. In the applications where a constant compressive preload and/or a cyclic mechanical load is applied, it may be argued that the low first cycle stiffness at small electric fields (Fig. 2(a)) is meaningless for actuator design. That is, higher stiffness values that are observed after reaching a steady stress–strain response (after several cycles with no residual strain) seem to be the only values important. However, these values would change if a sufficiently large electric field is subsequently applied. During normal operations where the applied electric field changes continuously, it will tend to realign the mechanically rotated domains towards the direction of applied electric field and thus eliminate the residual strain (and associated steady-state stress–strain response). To illustrate this better, the stress–strain response of Stack B as a function of mechanical cycles is shown in Fig. 3, before and after the application of electric field. Initially, low electric field was applied to the sample (0.28 MV/m), after which it was preloaded to 13.8 MPa (2 ksi) and cycled between 13.8 and 41.4 MPa (2 and 6 ksi) until a steady stress–strain response was observed (five cycles). Then, an electric field ($-$ min/$+$ max) was applied to the sample for several cycles while it was held at 13.8 MPa (2 ksi). Following this, another five mechanical cycles from 13.8 to 41.4 MPa (2 to 6 ksi) were applied to the sample. Young's modulus values before and after the application of electric field (strain reset) are shown in Fig. 3(b) as a function of mechanical cycles. It can be seen that, after the application of the electric field the stiffness values were reduced and followed the same path as during the initial loading. These results indicate that the low stiffness values associated with the first mechanical cycle (at low electric fields) cannot be neglected in structural applications. Finally, it should be pointed out that before each test described in this document, the piezoelectric stacks were cycled between minimum and maximum recommended electric field values for several cycles (strain reset), to cancel any residual strains present from the previous tests.

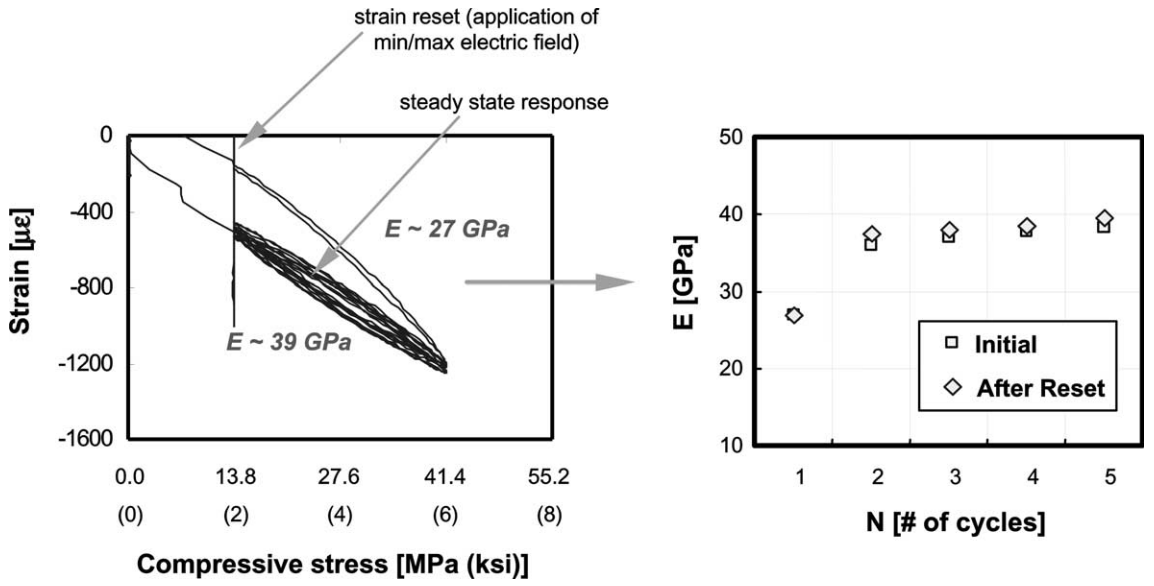

Fig. 3. Stress–strain response as a function of number of mechanical cycles (Stack B, electric field = 0.28 MV/m, five mechanical cycles from 13.8 to 41.4 MPa at 0.1 Hz).

2.2. Electrical loading under constant compressive preload

Electrical characterization tests were performed under different constant mechanical preloads. Properties were experimentally determined over a wide range of mechanical preloads 0–68.9 MPa (0–10 ksi). As in the case of mechanical loading, before each test a strain reset procedure was applied to cancel any residual strains present from the previous tests. Following this, samples were preloaded to a specified compressive stress (between 0 and 68.9 MPa) followed by the application of an alternating (sine wave) electric field (Table 1). Measurements were taken at three different frequencies of the applied electric field: 0.1, 1, and 10 Hz, and data was recorded for five electrical cycles. After the measurements were taken, compressive prestress was removed and the entire procedure was repeated for another value of applied preload (13.8 MPa increment).

An example of the voltage–strain response as a function of the applied preload is shown in Fig. 4 for Stack B. Strain output (piezoelectric coefficients) was determined by taking the difference between the maximum and minimum strain at each value of the applied preload. Data presented in Fig. 4 are for the electrical loading at 1 Hz. While the same trend in the voltage–strain behavior is observed for other cycling frequency, measurements indicate a small influence of frequency on the total strain output. That is, for electrical loading at 0.1 Hz, strain output was on the average 5% higher than at 10 Hz. At this time this results is regarded as inconclusive and tests at higher cycling frequencies are required to determine the exact influence of this parameter (i.e., frequency) on piezoelectric properties of stack actuators. This is important in determining the frequency at which domain motion occurs.

While the displacement output at different preloads is an important parameter, change in other properties as a function of the applied preload are also of interest for constitutive modeling and actuator applications. They include relative permittivity (e_r), electrical energy delivered to the actuator (U_E), mechanical energy delivered by the actuator (U_M), and the electro-mechanical coupling coefficients, k^2. Current output from the high-voltage amplifier was recorded during each test, and it was used to construct flux vs electric field diagrams for each value of the applied preload. This is schematically illustrated in Fig. 5, which also provides details on the data reduction procedure for calculating the electric flux (D). Slope of the flux–field curve is the

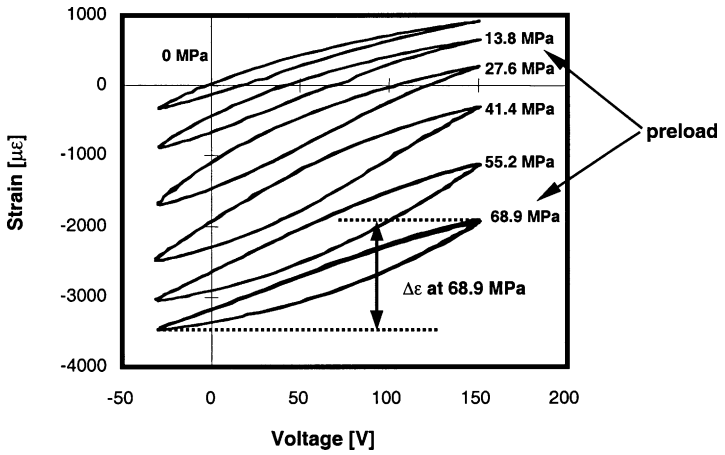

Fig. 4. Strain response as a function of applied preload: 0, 13.8, 27.6, 41.4, 55.2, and 68.9 MPa (Stack B at $f = 1$ Hz).

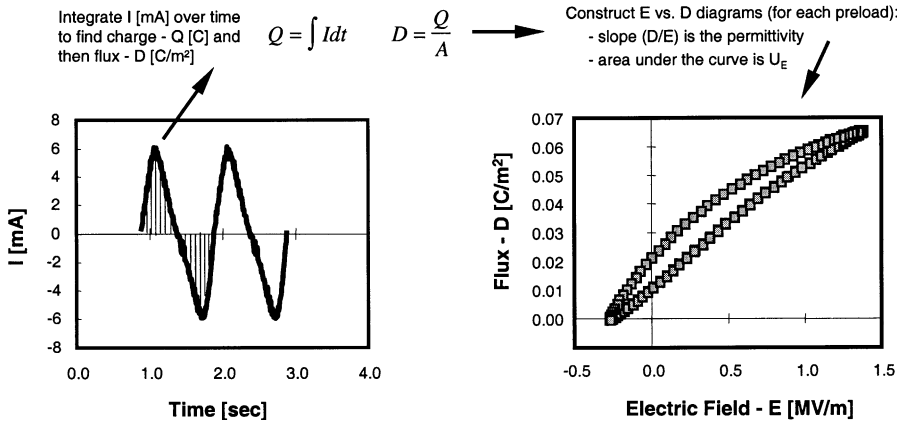

Fig. 5. Flux-field diagram: procedure for calculating relative permittivity, e_r, and input electrical energy density, U_E.

permittivity ($e = \Delta D/\Delta E,\ e_r = e/e_0$) while the area under the curve represents the electrical energy delivered to the system. This value was further normalized with respect to the density of the actuator (ρ) in order to compare the performance of stacks made from different materials, i.e.

$$U_E = \frac{1}{\rho}\left(\frac{1}{2}\Delta E\,\Delta D\right). \tag{1}$$

For these tests mechanical energy delivered by the actuator (mechanical energy density) was approximated through the relationship (note that the direct measurements are made during combined electromechanical loading)

$$U_M = \frac{1}{\rho}\left(\frac{1}{2}E\Delta\varepsilon^2\right), \tag{2}$$

where $\Delta\varepsilon$ is the strain output for each preload (Fig. 4), and E is Young's modulus evaluated in the vicinity of each preload value (i.e., preload ± 13.8 MPa (± 2 ksi)). However, it was shown in the previous section that stiffness of the actuator changes significantly as a function of applied electric field and mechanical loading

conditions. Since $\Delta\varepsilon$ was determined for one full electrical cycle (from minimum to maximum electric field), it was deemed appropriate to use the average value of Young's modulus to determine U_M. To determine the stiffness values over the broader range of electric field conditions, voltage–strain response at different preloads (Fig. 4) was used to reconstruct stress–strain diagrams for different values of applied voltage. These stress–strain curves were then used to determine Young's modulus at different voltages and load ranges for calculating mechanical energy (Eq. (2)). Detailed procedure is outlined in Mitrovic et al. (1999), and the stiffness values obtained in this manner were close to the first cycle stiffness observed during mechanical loading tests.

Different definitions and methods exist to calculate electro-mechanical coupling coefficient (Ikeda, 1990; Wise and Hooker, 1997), and some of the most commonly employed ones relate k to compliance at constant flux and field conditions ($1 - k^2 = S^D/S^E$). While this method could be applied in this study, since both open- and short-circuit compliance have been determined, we chose a more precise definition (Ikeda, 1990) which relates k to the stored mechanical energy and supplied electrical energy:

$$k^2 = \frac{U_M}{U_E}. \tag{3}$$

We choose this approach because under combined electro-mechanical loading S^D and S^E cannot easily be determined, while the input electrical energy and output mechanical energy can be directly measured, as explained in the following paragraphs.

2.3. Combined electro-mechanical loading (out of phase)

In the previous two sections, we described either mechanical loading at constant electric field or electrical loading at constant mechanical load. In this section, we describe cyclic electro-mechanical loading in which both electrical and mechanical load change simultaneously. Assuming that electrical and mechanical loading occur at the same frequencies, two extreme cases can be defined: in-phase and out-of-phase loading. An example of these two cases is shown in Fig. 6. In this study, we focus on out-of-phase electro-mechanical loading characterization because this is believed to represent a worst case operating scenario. As shown in Fig. 6, without a mechanical load (path 1–2) the actuator's strain output is ~1200 με. However, when an out-of-phase mechanical load is applied from 0 to 55.2 MPa (0 to 8 ksi) the actuator's strain response is completely impeded (path 1–3), i.e., zero strain output. The question is what are the electro-mechanical properties during this loading sequence and how are they related to properties determined during constant field (load) tests.

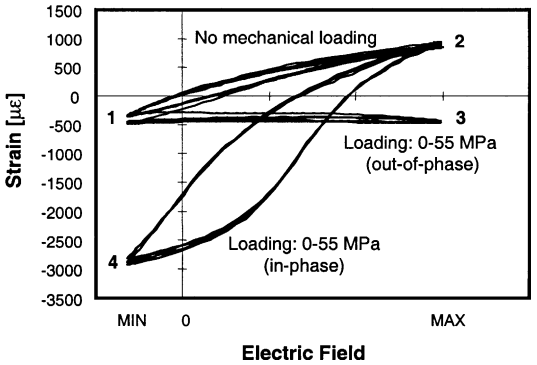

Fig. 6. Example of voltage–strain response under the combined electro-mechanical loading (in-phase and out-of-phase).

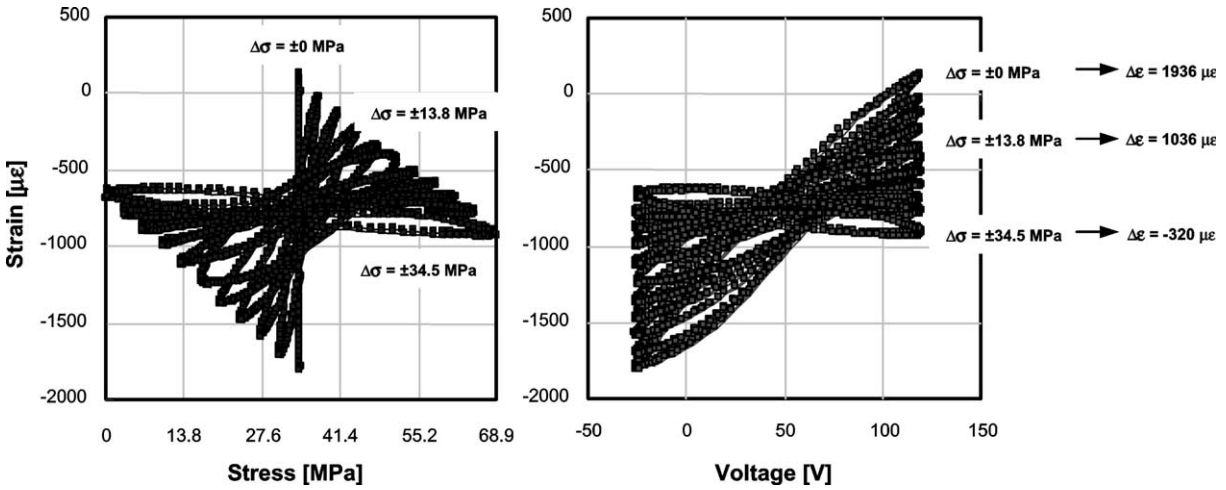

Fig. 7. Example of out-of-phase electro-mechanical loading constant preload: 34.5 MPa, variable load amplitude: ±3.4, ±6.9, ±10.3, ±13.8, ..., ±34.5 MPa.

To address this issue, a number of tests were performed in which both the mechanical prestress and stress amplitude were varied. Mechanical preload values were varied between 13.8 and 55.2 MPa (increment 6.9 MPa), while the range of load amplitudes was between ±3.4 and ±34.5 MPa (increment ±3.4 MPa). Initially, a constant preload was applied to the sample after which cyclic electric field was applied (recommended field range). Following that, mechanical load of different amplitudes was applied out of phase with electrical loading while recording data. The same procedure was repeated for other values of compressive preload and stress amplitudes for total of 48 tests for each stack (cyclic electric field values were kept constant).

An example of stress–strain and voltage–strain response under combined electro-mechanical loading is presented in Fig. 7 for one preload value (34.5 MPa) and different load amplitudes. As shown in this figure, electric field induced strain output of the actuator monotonically decreases with an increase in load amplitude, as expected, until mechanical loading completely eliminates the piezoelectric strain. In addition to strain output, changes in other parameters (U_E, U_M, and k^2) as a function of loading conditions were also investigated. Electrical energy density was calculated according to the same procedures outlined in the previous section (Eq. (1)). In the case of constant preload, mechanical energy delivered by the actuator was approximated through the relationship that relates actuator's stiffness and strain output (Eq. (1)). For the case of electro-mechanical loading we employ a different method to determine U_M. That is, it was directly determined from the stress–strain curves (area under the curve). Due to the hysteresis effect, there exist differences in U_M calculated from the loading and unloading curves. In this study, the average of these two values was calculated and reported in this document. However, in the linear case U_M can also be approximated by the following relationship:

$$U_M \approx \frac{1}{\rho}\left(\frac{1}{2}\Delta\sigma\Delta\varepsilon\right). \tag{4}$$

Energy densities for two stacks are shown in Fig. 8 for all ranges of preload values and load amplitudes investigated in this study. As indicated in this figure, maximum values for U_M occur for load amplitude between ±13.8 and ±17.2 MPa regardless of the value of applied preload. Similar behavior is observed for the other four piezoelectric stacks. Therefore, in the remainder of this study, we focus on the load amplitude of ±13.8 MPa as the optimum one, and present results for influence of applied preload on changes in strain

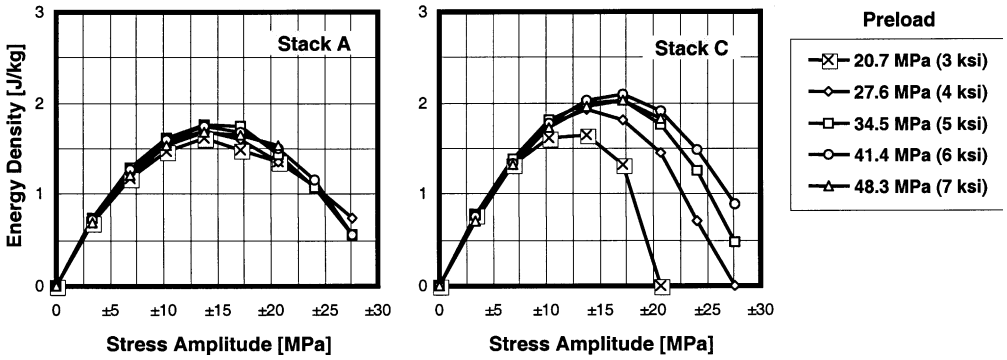

Fig. 8. Mechanical energy density as a function of preload and load amplitude.

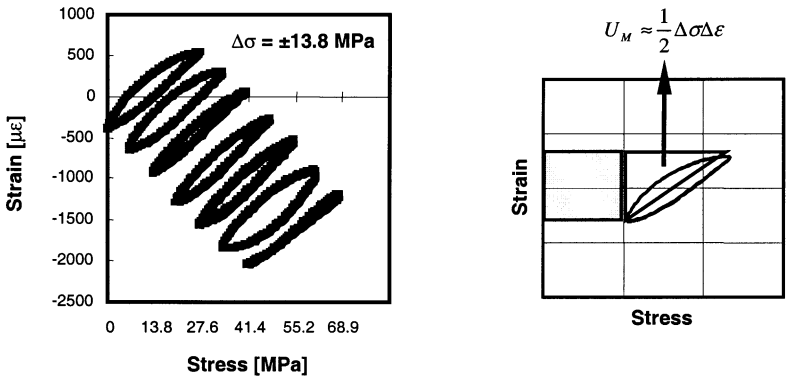

Fig. 9. Example of out-of-phase electro-mechanical loading for constant load amplitude (±13.8 MPa).

output, energy density, and coupling coefficients. An example of stress–strain response for this case is illustrated in Fig. 9, and on the right side of this figure, the procedure for calculating U_M is outlined. That is, only the area under the curve for which both stress and strain change (triangular area in Fig. 9) was included in the energy density calculations (Eq. (4)). We believe that this represents an accurate description of the mechanical energy delivered by the actuator. The rectangular portion under the stress–strain curve (Fig. 9) represents the work against the constant preload applied to the sample during the actuator assembly, and it cannot be considered as useful work for application that requires a preload. For other actuator applications, the complete area under the stress–strain curve (both triangular and rectangular portions) may be considered as the energy delivered by the actuator. Energy density and coupling coefficients calculated using both approaches for one stack (based on data presented in Fig. 9) are shown in Table 2.

3. Results and discussion

As indicated in the previous sections, elastic and piezoelectric properties of stack actuators were evaluated at different frequencies: at 0.1, 1, 10, and 40 Hz in the case of mechanical loading; at 0.1, 1, and 10 Hz under electrical loading; and at 0.1 and 1 Hz under combined electro-mechanical loading. While a slight decrease in piezoelectric properties was observed due to the increase in electrical loading frequency, mechanical properties were shown to be less sensitive to changes in loading frequency. To compare the performance of different stack actuators we present only the results for a specific cycling frequency (1 Hz)

Table 2
Mechanical energy density and coupling coefficients using different methods for calculating U_M (example: Stack A)

Preload (MPa)	U_M[a] (J/kg)	U_M[b] (J/kg)	U_E (J/kg)	k^{2a}	k^{2b}
13.8	1.69	1.69	7.27	0.23	0.23
20.7	1.73	2.59	7.68	0.23	0.34
27.6	1.83	3.65	8.13	0.22	0.45
34.5	1.86	4.64	8.76	0.21	0.53
41.4	1.87	5.61	9.10	0.21	0.62
48.3	1.73	6.06	9.43	0.18	0.64
55.2	1.58	6.32	9.48	0.17	0.67

[a] $U_M = \frac{1}{2}\Delta\sigma\Delta\varepsilon$.
[b] Full area.

which was common for all three loading scenarios. Therefore, in the following paragraphs, elastic and piezoelectric properties of six stack actuators evaluated at 1 Hz are compared for mechanical, electrical, and combined electro-mechanical loading scenario.

3.1. Mechanical properties

In the following paragraphs, we compare stiffness data of the six stacks measured from mechanical loading tests performed at short-circuit conditions (after 1 and 10 cycles, see Section 2.1 and (Fig. 2(a)). Stiffness properties obtained in this fashion provide upper and lower bounds. This is because at the first mechanical cycle the stiffness is a function of domain wall motion, i.e., stiffness in the polarization direction. At the later stage of loading (i.e., ~10th cycle) we are approaching the stiffness in the 90° direction which is higher than in the polarization direction. In Fig. 10, Young's modulus values (E) are shown as a function of the mechanical operating load range and number of mechanical cycles (first and 10th cycle stiffness, short-circuit condition). Results indicate that, depending on the operating load range, Young's modulus can change by more than 100% for certain stack actuators. This is especially prominent for PLZT based actuators (Stacks C and D), which are very compliant in the initial load range (0–2 ksi) and become stiffer as the applied load increases (8–10 ksi). On the other hand, actuators made from PZT materials (Stacks A, B, E, and F) generally displayed higher stiffness at the lower preloads. These differences are mainly attributed to different material compositions. However, other parameters, such as the stiffness of the bond line and electrode layers, can play a role in the overall stack's mechanical response. However, it is out of the scope of this paper to investigate these later issues of lesser importance.

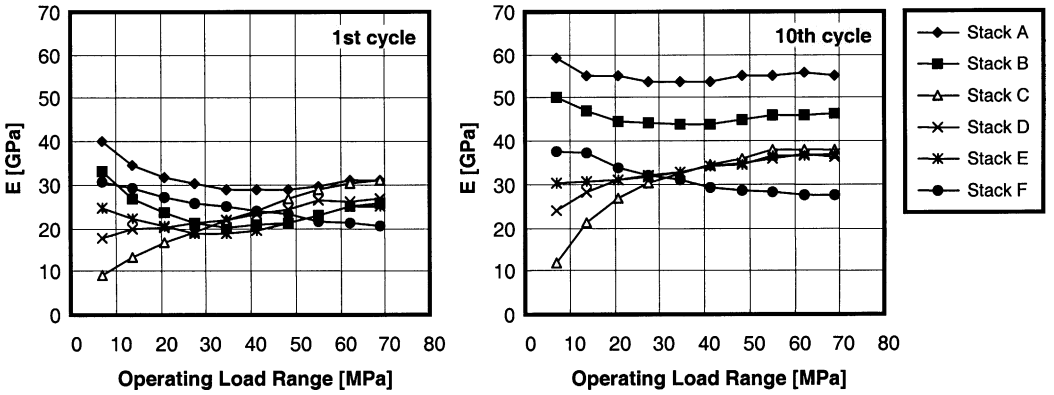

Fig. 10. Young's modulus as a function of mechanical loading conditions (operating stress range and number of mechanical cycles).

The method used to measure stiffness properties of stack actuators can also play a significant role in characterizing the mechanical response. As mentioned earlier, stiffness values presented in this section provide both lower and upper bounds of this property. Young's modulus values reported by stack manufacturers fall on the higher end of measured stiffness values, such as the E evaluated at high electric fields (Fig. 2(b)) and/or when the steady state response is achieved (Fig. 10(b)). These discrepancies are attributed to different experimental methods used to evaluate mechanical properties of stack actuators. However, due to the influence of electro-mechanical operating conditions on mechanical properties, defining only one value for Young's modulus is inappropriate in structural applications where piezoelectric actuators are subjected to a wide range of mechanical loads.

3.2. Properties under constant preload

Properties of piezoelectric stacks for electrical loading under different values of applied compressive stress are outlined in Figs. 11–13. It is evident that the magnitude of the applied preload significantly influences strain output, electrical and mechanical energy density, and coupling coefficients. Influence of the applied preload on piezoelectric properties is shown in Fig. 11. The results presented in this figure indicate similar trend in the piezoelectric response vs preload for all six actuators. That is, the strain output is initially enhanced with an increase in mechanical preload. The maximum strain values are obtained when the stacks are preloaded between 25 and 40 MPa. At higher preloads, the overall piezoelectric extrinsic effect is impeded causing the strain to decrease. Zhang et al. (1994) provided evidence that at room temperature the large piezoelectric response of PZT materials is mainly due to non-180° domain wall motion (extrinsic properties). Domain wall motion can be managed either with mechanical load or with electrical field. That is, when the nominal compressive stress is applied to the sample these domains tend to align perpendicular to the loading direction. Upon the application of sufficiently large electric field, domains will be forced to re-orient towards the loading direction thus enhancing the overall strain output above the intrinsic properties. However, whether the piezoelectric properties will be enhanced or reduced depends on both the magnitude of applied mechanical load as well as the electric field values.

In this study, PZT-5H and PZT-5A materials as well as PLZT compositions were investigated, with results indicating similar behavior (piezoelectric response vs preload). Hackenberger et al. (1998) reported similar results on properties of PZT-5H equivalent material (TRS600FG). Other researchers also reported an increase in the overall strain response with an increase in uniaxial stress for PLSnZT compositions (Pan et al., 1998). However, in another study (Wise and Hooker, 1997) a decrease in displacement upon the application of load was observed for four different piezoelectric stacks including PZT-5H type of material.

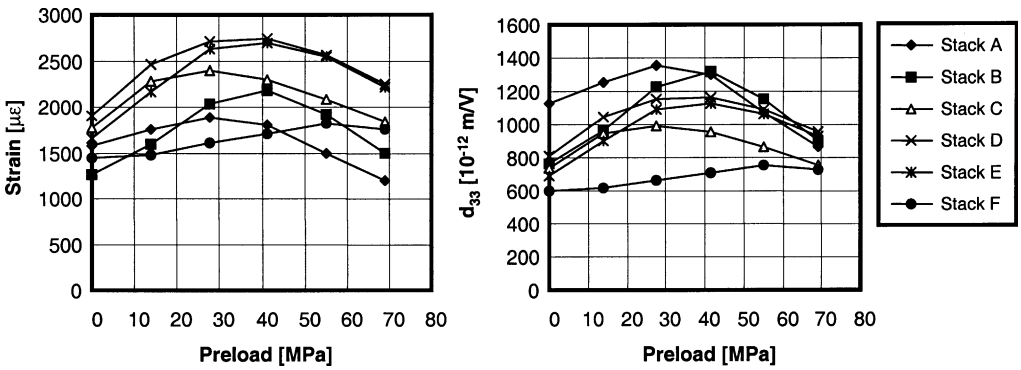

Fig. 11. Piezoelectric properties as a function of applied mechanical preload.

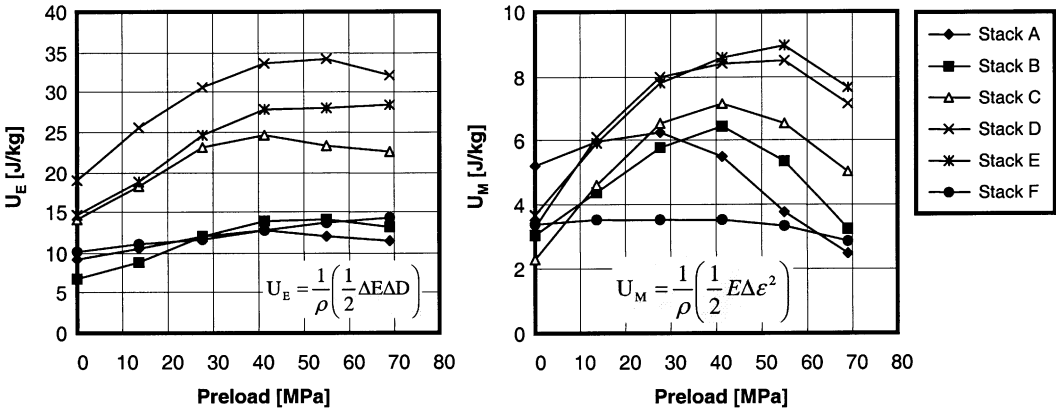

Fig. 12. Electrical and mechanical energy density as a function of applied mechanical preload.

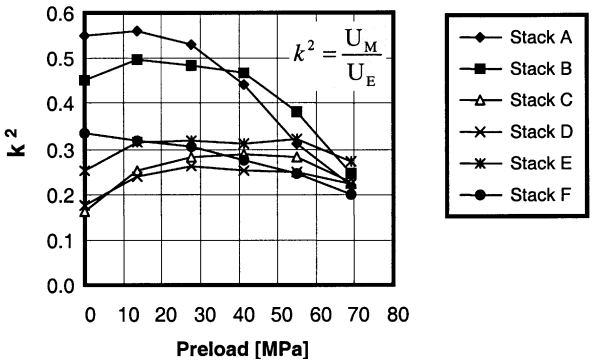

Fig. 13. Coupling coefficients as a function of applied mechanical preload.

Also, for TRS200FG material (PZT-5A equivalent) strain output was reported to continually decrease with the applied stress (Hackenberger et al., 1998). These results reinforce the notion that the piezoelectric properties are strongly dependent upon electro-mechanical loading conditions and the type of material being considered. Therefore, the results presented here are valid for specified electric field and mechanical load ranges.

Data presented in Fig. 11 indicates that an optimum preload range exists to maximize the strain output of the actuator. The increase in strain output at a preload of between 25 and 40 MPa can be quite significant when compared to the free stroke strain (0 MPa). This increase ranges between 20% for Stack A to 70% for Stack B. Strain values between 1800 $\mu\varepsilon$ (Stack F) and 2700 $\mu\varepsilon$ (Stack E) can be achieved for this operating region. While data in Fig. 11(a) indicate that Stacks D and E have the best performance in terms of the strain output, different conclusions can be reached when comparing piezoelectric coefficients d_{33} (Fig. 11(a)). These non-linear piezoelectric coefficients were determined by dividing the maximum strain by the electrical operating field. Stacks A and B show the highest values of piezoelectric coefficients due to the fact that they were operated at relatively lower electric field values (see Table 1 for manufacturer's recommended field values).

Influence of the applied preload on mechanical and electrical energy density is shown in Fig. 12. It should be noted that U_M in Fig. 12(b) is predicted (Eq. (2)) and not directly measured. Mechanical energy

density (Fig. 12(b)) follows a similar trend observed for the variation in strain output as a function of the applied preload (Fig. 11(a)). This is an expected result since mechanical energy density depends mainly on the strain output ($\Delta\varepsilon$) as well as on the stiffness of the actuator (Eq. (2)). In this case, the optimum preload values for Stacks D and E are shifted to larger values of applied preload (41.4–55.2 MPa) due to the higher stiffness values of these actuators for this load range (Fig. 10). An increase in the applied preload is also accompanied with an increase in electrical energy required to drive these actuators (Fig. 12(a)). That is, higher electrical energy input is needed to overcome the applied mechanical load. However, above 41.4 MPa preload, the electrical energy density reaches a maximum value and remains almost constant upto a preload of 68.9 MPa, indicating that no further enhancement in the strain output is achieved. Stacks A and B required the lowest electrical energy input, mainly due to the lower operating electric field range. Therefore, electro-mechanical coupling coefficients, k, for these two stacks are substantially higher than for other four stacks, especially for the lower values of applied preload (Fig. 13). However, at higher preloads (55.2–68.9 MPa) differences in coupling coefficients between the six stacks diminish leading to very similar coupling properties.

The general trend in data suggest that for piezoelectric stacks evaluated in this study optimum values of the applied preload (i.e., maximum domain wall motion) are between 25 and 40 MPa. However, it should be also noted that the increase in actuation capability with compressive prestress is also accompanied with a larger hysteresis (Fig. 4) arising from domain wall motion. This can potentially lead to excessive heat generation under long-term electro-mechanical loading and to possible degradation in piezoelectric properties. Therefore, fatigue effects must also be addressed to fully characterize the electro-mechanical response of piezoelectric stack actuators, and to determine the optimum operating conditions under which they should be operated.

3.3. Properties under combined electro-mechanical loading

As indicated in Section 2.3, the mechanical loading amplitude of ±13.8 MPa (±2 ksi) produced the highest mechanical energy density under combined out-of-phase electro-mechanical loading. Therefore, in the following paragraphs, we present results for changes in strain output, energy density, and coupling coefficients, for a fixed value of cyclic load amplitude (±13.8 MPa). We reiterate that these properties were all directly measured. Relationships between these properties are shown in Figs. 14 and 15. Note that since load amplitude was held constant, mechanical energy density follows the same trend as the strain output

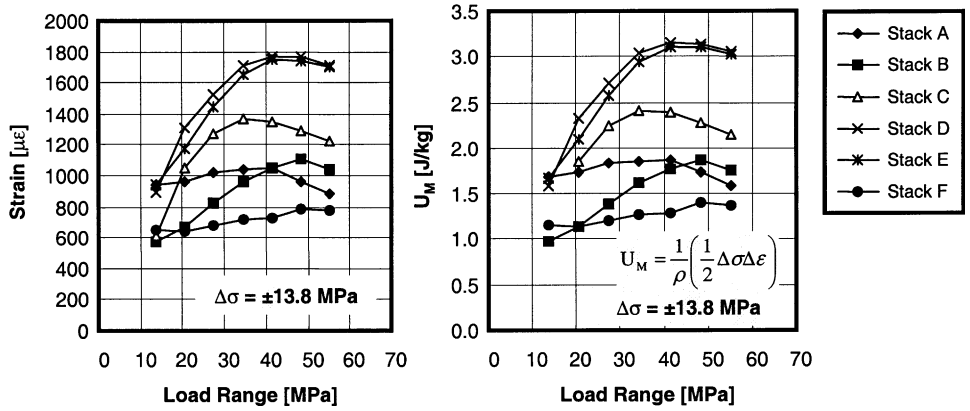

Fig. 14. Strain output and mechanical energy density as a function of applied mechanical preload for specific value of load amplitude: ±13.8 MPa (±2 ksi).

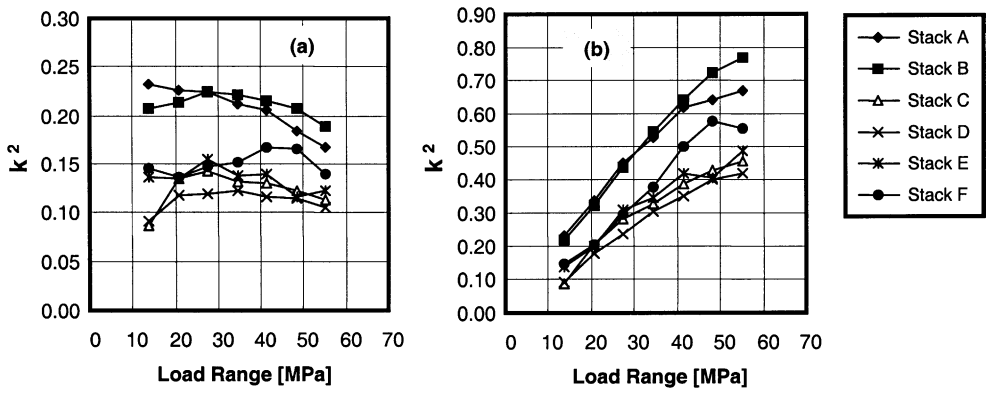

Fig. 15. Coupling coefficients as a function of applied mechanical preload (i.e., mean stress) for specific value of load amplitude: ±13.8 MPa (±2 ksi).

(Eq. (4)). Strain and energy density values under the combined electro-mechanical loading are lower than in the case of constant preload. However, despite the variable mechanical load of ±13.8 MPa, maximum available strain output is between 780 and 1750 με for different piezoelectric stacks. For this loading scenario optimum preload values are between 35 and 48 MPa (5 and 7 ksi), similar to the results obtained from constant preload tests. Also, Stacks D and E have the best performance in terms of the strain output and energy density, while Stacks A and B displayed the lowest energy requirements and highest coupling coefficients (Fig. 15). In this figure coupling coefficients, calculated using two approaches described in Section 2.3 and shown in Table 2, are presented. Changes in coupling properties as a function of operating load range show different trends (and values) depending on the approach used to evaluate this property. The approach that includes work against variable load and neglects work against the applied constant preload (Section 2.3 and U_M in Fig. 14(b)) leads to almost uniform values of k^2 over the range of compressive loads investigated. On the other hand, if the energy delivered by the actuator includes work against the constant preload, an increase in k^2 is measured at higher preloads (55.2 ± 13.8 MPa, 8 ± 2 ksi). Values as high as 0.78 have been measured. While the higher values of compressive loads were not the topic of this study, it is expected that the values of mechanical energy delivered by the actuator (and subsequently coupling coefficient) will decrease for larger mechanical loads that impede the piezoelectric effect.

While the results under combined electro-mechanical loading show similarities with the data from constant amplitude tests, there are very important differences between these two loading scenarios. This issue raises the question if we can predict combined electro-mechanical response (EM) based on data obtained from mechanical loading tests at different electric field values ($E = \text{const}$) and electrical loading tests at different preloads ($\sigma = \text{const}$). In Fig. 16, measured strain output for each stack under combined electro-mechanical loading is compared to predicted values based on strain outputs obtained from constant preload tests and expected reduction in strain due to the mechanical loading (±13.8 MPa). Eq. (5) was used to evaluate the response under the combined loading scenario. Since stiffness values change significantly depending on electro-mechanical conditions both first and 10th cycle compliance, S, were used in constructing data presented in Fig. 16.

$$\varepsilon_{33}^{\mathrm{EM}} = \sigma_{33} S_{33}^{\mathrm{E}=\mathrm{const}} + E d_{33}^{\sigma=\mathrm{const}}. \tag{5}$$

Data in Fig. 16 indicate that linear superposition of mechanical and electrical strain outputs provides bounds on the response under combined electro-mechanical loading. However, it still does not lead to accurate predictions over a broad range of loading conditions. Differences between predicted and measured strain values for certain load ranges can be quite high (upto 35% if first cycle compliance is used and upto

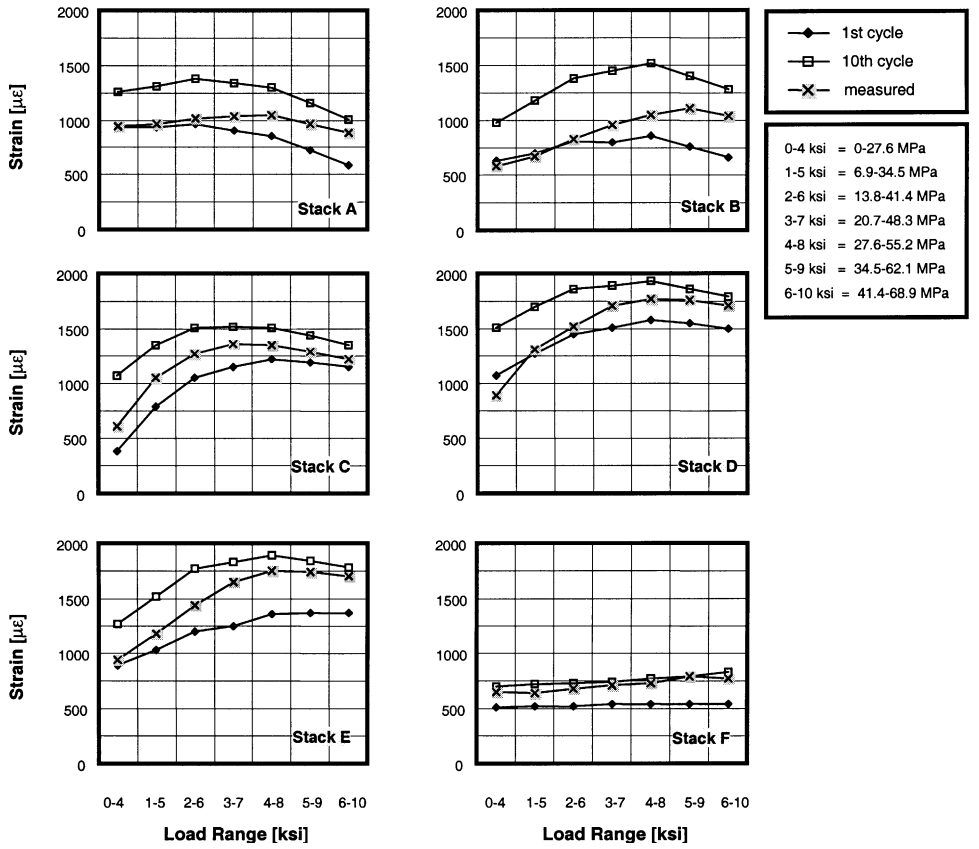

Fig. 16. Comparison of measured strain output under combined out-of-phase electro-mechanical loading (for specific value of load amplitude: ±13.8 MPa) and predicted strain output based on linear approaches.

70% for 10th cycle compliance). Furthermore, data presented in Fig. 16 generally shows better correlation when first cycle compliance is used for lower values of compressive stress (except for Stack F), while for higher values of applied load 10th cycle compliance provides better results. Such behavior might be attributed to the method in which the actuator stiffness is measured from mechanical loading tests (Sections 2.1 and 3.1). That is, stiffness values shown in Fig. 10 are determined from tests performed from 0 to 69 MPa and without applied electric field (short-circuit conditions). However, during combined electro-mechanical loading, the electric field is not held constant and it varies between −0.4 and 2 MV/m for certain actuators. Also, the range of mechanical loads was different for stiffness measurement tests and under the combined loading scenario. These two issues (i.e., electric field and mechanical load) suggest that in order to accurately predict the response under combined electro-mechanical loading, measurements should be made at comparable loading conditions.

Experimental data presented in this paper indicate that loading conditions strongly influence the properties of piezoelectric material. The question that arises is what are the regions of both mechanical and electrical load for which a stack actuator can be modeled as having constant elastic and piezoelectric properties. This is not only important for combined (variable) electro-mechanical loading, but also for choosing the appropriate piezoelectric properties when the material is subjected to constant mechanical load (Section 3.2). Conclusion regarding the optimum preload that produces largest strain output is valid only for the range of electric fields investigated in this study (upto 2 MV/m). That is, if the piezoelectric

actuators are used at very low electric field levels (~0.5 MV/m) electrical energy supplied to the actuator might not be sufficient to overcome the applied mechanical load leading to the steady decrease in d_{33} with an increase in applied load. It should be noted that it is possible to capture some of the non-linear behavior reported in this paper by using the piecewise linear model coupled with a switching criteria as explained by Fotinich (2000). However, there is still a need to better understand and model non-linear processes that occur under the combined electro-mechanical loading.

4. Summary

The influence of electro-mechanical operating conditions on the actuation capabilities of six piezoelectric stack actuators was investigated in this study. Experimental results indicate strong dependence of both elastic and piezoelectric properties on the operating conditions (mechanical and electrical). Young's modulus values of piezoelectric stacks were found to change significantly as a function of the applied electric field, as well as the mechanical loading range. Piezoelectric coefficients and the energy density delivered by the actuator initially increase upon the application of mechanical compressive stress. However, applying a higher preload has the adverse effect on the stacks response since mechanical loading impedes domain wall motion reducing the overall strain output. Maximum values of these properties are obtained when the stacks are preloaded between 25 and 40 MPa. Under combined out-of-phase electro-mechanical loading, optimum prestress values and mechanical loading amplitude leading to the highest energy density are 35–48 and ±13.8 MPa, respectively. However, it should be noted that the increase in actuation capability with the application of compressive prestress is also accompanied with a larger hysteresis arising from the domain wall motion. This can potentially lead to excessive heat generation under the long-term electro-mechanical loading and to possible degradation in piezoelectric properties. Therefore, the fatigue effects must also be addressed to fully characterize the electro-mechanical response of piezoelectric stack actuators, and to determine the optimum operating conditions under which they should be operated. Finally, the results of this study indicate that linear superposition of properties from constant field/load tests can be used to bound combined electro-mechanical response but the bounds are quite large.

Acknowledgements

DARPA and the Army Research Office (ARO) supported the vast majority of this work. The DARPA support is under Agreement MDA972-98-3-0001 with Dr. Ephrahim Garcia as the DARPA program manager and Dr. Gary Anderson as the technical monitor from the US Army Research Office. The ARO support is under contract number DAAH04-95-1-0095 with John Prater as the contract monitor. The support and guidance of both agencies is sincerely appreciated. In addition to this support, the principal investigators received financial support from NASA-Dryden contract monitor Lance Richards.

References

Chen, Q., Yao, D.-J., Kim, C.-J., Carman, G.P., 1998. Frequency response of an inchworm motor fabricated with micro machined interlocking surface, mesoscale actuator device. Proceedings of SPIE, Smart Structures and Integrated Systems, vol. 3329, pp. 768–779.

Fotinich, Y., 2000. Nonlinear Modeling of Piezoceramics. Ph.D. Dissertation, University of California, Los Angeles.

Friedman, P.P., Millott, T.A., 1995. Vibration reduction in rotorcraft using active control: a comparison of various approaches. Journal of Guidance, Control, and Dynamics 18 (4), 664–673.

Giurgiutiu, V., Chaudhry, Z., Rogers, C.A., 1995. Energy-Based Comparison of Solid-State Actuators. Report no. CIMSS 95-101, Virginia Polytechnic Institute and State University.

Hackenberger, W., Pan, M.-J., Vedula, V., Pertsch, P., Cao, W.-W., Randall, C., Shrout, T., 1998. Effect of grain size on actuator properties of piezoelectric ceramics. Proceedings of SPIE, Smart Materials Technologies, vol. 3324, pp. 28–36.

Ikeda, T., 1990. Fundamentals of Piezoelectricity. Oxford University Press, Oxford, UK.

Lee, T., Chopra, I., 1998. Design and static testing of a trailing-edge flap actuator with piezostacks for a rotor blade. Proceedings of SPIE, Smart Structures and Integrated Systems, vol. 3329, pp. 321–332.

Mitrovic, M., Carman, G.P., Straub, F.K., 1999. Electro-mechanical characterization of piezoelectric stack actuators. Proceedings of SPIE, Smart Structures and Integrated Systems, vol. 3668, pp. 586–601.

Pan, M.-J., Pertsch, P., Yoshikawa, S., Shrout, T.R., Vedula, V., 1998. Electroactive actuator materials: investigations on stress and temperature characteristics. Proceedings of SPIE, Smart Materials Technologies, vol. 3324, pp. 145–153.

Park, S.-E., Vedula, V., Pan, M.-J., Hackenberger, W.S., Pertsch, P., Shrout, T.R., 1998. Relaxor based ferroelectric single crystals for electromechanical actuators. Proceedings of SPIE, Smart Materials Technologies, vol. 3324, pp. 136–144.

Prechtl, E.F., Hall, S.R., 1998. An X-frame actuator servo-flap actuation system for rotor control. Proceedings of SPIE, Smart Structures and Integrated Systems, vol. 3329, pp. 309–320.

Straub, F.K., Merkley, D.J., 1995. Design of a smart material actuator for rotor control. Proceedings of SPIE, Smart Structures and Integrated Systems, vol. 2443, pp. 89–104.

Sumali, H., Cudney, H., Vipperman, J., 1992. Vibration control of cylinders using piezoelectric sensors and actuators. Proceedings of DPA/AIAA/ASME/SPIE, Active Materials and Adaptive Structures, pp. 467–472.

Wang, D., Fotinich, Y., Carman, G.P., 1998. Influence of temperature on the electro-mechanical and fatigue behavior of piezoelectric ceramics. Journal of Applied Physics 83 (10), 5342–5350.

Wise, S.A., Hooker, M.W., 1997. Characterization of Multilayer Piezoelectric Actuators for use in Active Isolation Mounts. NASA Technical Memorandum 4742.

Zhang, Q.M., Wang, H., Kim, N., Cross, L.E., 1994. Direct evaluation of domain-wall and intrinsic contributions to the dielectric and piezoelectric response and their temperature dependence on lead zirconate–titanate ceramics. Journal of Applied Physics 75 (1), 454–459.